Structure of a Protozoan Virus from the Human Genitourinary Parasite *Trichomonas vaginalis*

Kristin N. Parent,[a]* Yuko Takagi,[b] Giovanni Cardone,[a] Norman H. Olson,[a] Maria Ericsson,[c] May Yang,[b] Yujin Lee,[d] John M. Asara,[e,f] Raina N. Fichorova,[d,e] Timothy S. Baker,[a,g] Max L. Nibert[b]

Department of Chemistry & Biochemistry, University of California, San Diego, La Jolla, California, USA[a]; Department of Microbiology & Immunobiology[b] and Electron Microscopy Facility,[c] Harvard Medical School, Boston, Massachusetts, USA; Laboratory of Genital Tract Biology, Department of Obstetrics, Gynecology, and Reproductive Biology, Brigham and Women's Hospital, Boston, Massachusetts, USA[d]; Department of Medicine, Harvard Medical School, Boston, Massachusetts, USA[e]; Division of Signal Transduction, Beth Israel Deaconess Medical Center, Boston, Massachusetts, USA[f]; Division of Biological Sciences, University of California, San Diego, La Jolla, California, USA[g]

* Present address: Kristin N. Parent, Department of Biochemistry & Molecular Biology, Michigan State University, East Lansing, Michigan, USA.

K.N.P. and Y.T. contributed equally to this article.

ABSTRACT **The flagellated protozoan *Trichomonas vaginalis* is an obligate human genitourinary parasite and the most frequent cause of sexually transmitted disease worldwide. Most clinical isolates of *T. vaginalis* are persistently infected with one or more double-stranded RNA (dsRNA) viruses from the genus *Trichomonasvirus*, family *Totiviridae*, which appear to influence not only protozoan biology but also human disease. Here we describe the three-dimensional structure of Trichomonas vaginalis virus 1 (TVV1) virions, as determined by electron cryomicroscopy and icosahedral image reconstruction. The structure reveals a $T = 1$ capsid comprising 120 subunits, 60 in each of two nonequivalent positions, designated A and B, as previously observed for fungal *Totiviridae* family members. The putative protomer is identified as an asymmetric AB dimer consistent with either decamer or tetramer assembly intermediates. The capsid surface is notable for raised plateaus around the icosahedral 5-fold axes, with canyons connecting the 2- and 3-fold axes. Capsid-spanning channels at the 5-fold axes are unusually wide and may facilitate release of the viral genome, promoting dsRNA-dependent immunoinflammatory responses, as recently shown upon the exposure of human cervicovaginal epithelial cells to either TVV-infected *T. vaginalis* or purified TVV1 virions. Despite extensive sequence divergence, conservative features of the capsid reveal a helix-rich fold probably derived from an ancestor shared with fungal *Totiviridae* family members. Also notable are mass spectrometry results assessing the virion proteins as a complement to structure determination, which suggest that translation of the TVV1 RNA-dependent RNA polymerase in fusion with its capsid protein involves −2, and not +1, ribosomal frameshifting, an uncommonly found mechanism to date.**

IMPORTANCE ***Trichomonas vaginalis* causes ~250 million new cases of sexually transmitted disease each year worldwide and is associated with serious complications, including premature birth and increased transmission of other pathogens, including HIV. It is an extracellular parasite that, in turn, commonly hosts infections with double-stranded RNA (dsRNA) viruses, trichomonasviruses, which appear to exacerbate disease through signaling of immunoinflammatory responses by human epithelial cells. Here we report the first three-dimensional structure of a trichomonasvirus, which is also the first such structure of any protozoan dsRNA virus; show that it has unusually wide channels at the capsid vertices, with potential for releasing the viral genome and promoting dsRNA-dependent responses by human cells; and provide evidence that it uses −2 ribosomal frameshifting, an uncommon mechanism, to translate its RNA polymerase in fusion with its capsid protein. These findings provide both mechanistic and translational insights concerning the role of trichomonasviruses in aggravating disease attributable to *T. vaginalis*.**

Received 23 January 2013 **Accepted** 27 February 2013 **Published** 2 April 2013

Citation Parent KN, Takagi Y, Cardone G, Olson NH, Ericsson M, Yang M, Lee Y, Asara JM, Fichorova RN, Baker TS, Nibert ML. 2013. Structure of a protozoan virus from the human genitourinary parasite *Trichomonas vaginalis*. mBio 4(2):e00056-13. doi:10.1128/mBio.00056-13.

Editor Vincent Racaniello, Columbia University College of Physicians & Surgeons

Address correspondence to Timothy S. Baker, tsb@ucsd.edu and Max L. Nibert, mnibert@hms.harvard.edu.

The flagellated protozoan *Trichomonas vaginalis* is an obligate extracellular parasite of the human genitourinary mucosa (1). It is the most frequent cause of sexually transmitted disease worldwide and is associated with a variety of serious complications, including premature delivery, low birth weight, and increased transmission of other pathogens, including HIV and human papillomavirus (2). Clinical *T. vaginalis* isolates are often themselves persistently infected with dsRNA viruses, called Trichomonas vaginalis viruses (TVVs), from the genus *Trichomonasvirus*, family *Totiviridae* (3–8). Three species (abbreviated TVV1 to TVV3) are formally recognized (9, 10), and strains of a putative fourth have been reported (8). Moreover,

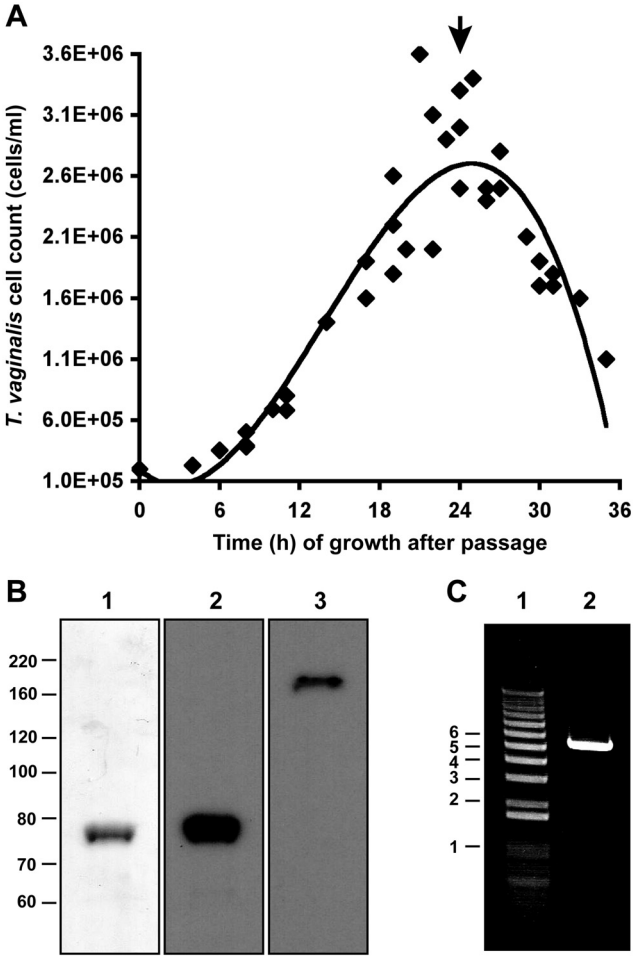

FIG 1 Growth of *T. vaginalis* isolate UH9 and components of purified TVV1-UH9 virions. (A) Aliquots were harvested from the growing culture at selected times after it was diluted into fresh medium at time 0 h. The concentration of cells in each aliquot (filled diamonds) was determined immediately after harvesting with an automatic cell counter. A best-fit curve for the data is also shown. The arrow indicates the time when such cultures were either diluted in fresh medium for passage or harvested by centrifugation for purification of virions. (B) Purified virions were disrupted by heating and run in different lanes of an 8% polyacrylamide gel. One lane was stained with Coomassie R-250 (lane 1). Protein molecular mass markers (kDa) were also analyzed, and their positions are shown at the left. The remainder of the gel was blotted to a membrane and probed with rabbit polyclonal antibodies that were raised against portions of the CP or RdRp region after expression in *Escherichia coli*. Antibody-bound CP (lane 2) and CP/RdRp (lane 3) bands were visualized by enhanced chemiluminescence. (C) Nondenaturing gel of the TVV genome. Nucleic acid contents of purified virions were extracted by phenol-chloroform-isoamyl alcohol and run in one lane of a 0.7% agarose gel (lane 2). DNA molecular size markers (kbp) were also analyzed (lane 1) as labeled at left.

coinfections of *T. vaginalis* isolates with two or more TVV species are common (8, 11–13).

The wide range of protozoan pathogens that host persistent infections with dsRNA viruses (e.g., *Cryptosporidium*, *Giardia*, and *Leishmania* in addition to *Trichomonas* [14–16]) suggests that they influence parasite biology and possibly human disease as well. Previous studies have shown that TVV infection is associated with variable expression of the *T. vaginalis* major surface antigen P270, which may aid the parasite in evading human adaptive responses (9, 17, 18). The presence of TVV has also been shown to decrease *T. vaginalis* growth or viability and to increase cysteine protease levels, either of which might alter pathogenesis in the human host (19). A few case studies comparing different aspects of trichomoniasis with the presence of TVV in *T. vaginalis* clinical isolates have noted correlations with patient signs and symptoms, but the case numbers have remained small (5, 13, 20).

In 2011, a pioneering report showed the influence of Leishmania RNA virus 1 (LRV1) on the pathogenesis of mucocutaneous leishmaniasis in a mouse model, providing definitive evidence of the role of that virus as a virulence factor in mammalian disease (21). Specifically, LRV1 in disseminating *Leishmania* cells induced immunoinflammatory cytokines and chemokines that promoted parasite persistence in infected mice. Recently, we provided similar evidence for TVV in a human disease model (22). In particular, similarly to LRV1 in the mouse model (21), we showed that TVV enhances immunoinflammatory responses to *T. vaginalis*. In human cervicovaginal epithelial cells, the natural host of *T. vaginalis*, both TVV-infected parasites and purified TVV virions triggered dsRNA-dependent type I interferon responses, as well as a number of proinflammatory mediators and chemokines (22), implicated in the pathogenesis of human trichomoniasis and its complications (1).

In light of the apparent role of TVV in exacerbating disease, a more complete understanding of its fundamental characteristics may be useful for improving both diagnostics and therapeutics of *T. vaginalis* infections. For each TVV species, the genome comprises a single, linear molecule of dsRNA 4.6 to 5.0 kbp long (8, 9, 12, 23, 24). The plus-strand RNA includes two long open reading frames (ORFs), an upstream one encoding the coat protein (CP) and a partially overlapping downstream one encoding the RNA-dependent RNA polymerase (RdRp). Ribosomal frameshifting is required for RdRp expression as part of a CP/RdRp fusion, which is incorporated in 1 or 2 copies per virion (25). The CP ranges from 678 to 746 amino acids (aa) (74 to 82 kDa), and the CP/RdRp ranges from 1,429 to 1,481 aa (159 to 165 kDa). Among the strains of a particular TVV species, the range of genome and protein sizes is much smaller (8). When viewed by negative-stain transmission electron microscopy (TEM), TVV virions are isometric and ~350 Å in diameter (3, 12, 26). Although the RNA replication cycle remains poorly characterized, it is presumed to be like that of other *Totiviridae* family members, including conservative transcription by the virion-associated CP/RdRp molecule(s) (27). Also like most other *Totiviridae* family members, TVVs lack the inherent means for extracellular transmission and are transmitted instead by direct cell-to-cell means during cytokinesis and perhaps mating (28).

One type of data that has remained unavailable for TVVs, as well as for other protozoan dsRNA viruses, is a three-dimensional (3D) structure of virions. Here we describe the 3D structure of TVV1 virions as determined by cryo-TEM and icosahedral image reconstruction. Among findings of special note are unusually large channels at the capsid vertices, which may facilitate release of the viral genome, promoting dsRNA-dependent immunoinflammatory responses, as recently shown for human epithelial cells exposed to either TVV-positive *T. vaginalis* isolates or purified TVV virions (22). Via mass spectrometry assessing the virion proteins as a complement to structure determination, we additionally provide evidence that translation of the TVV1 CP/RdRp protein

involves −2, and not +1, ribosomal frameshifting, an uncommonly found mechanism to date.

RESULTS

Initial characterizations of TVV1 virions used for structure studies. *T. vaginalis* isolate UH9 was chosen for use here because it is infected only with TVV1, unlike many other isolates that are coinfected with two to four TVVs (8). Moreover, both *T. vaginalis* UH9 and purified TVV1-UH9 virions have been shown to induce robust immunoinflammatory responses in human epithelial cells (22). *T. vaginalis* UH9 was serially passaged in liquid batch culture so that it ended exponential growth ~24 h after the preceding passage (Fig. 1A). On harvest day, cell pellets were sonicated to release virions, centrifuged to deplete debris, and then sedimented through a CsCl gradient. The gradient was fractionated, and fractions containing virions were identified by electrophoresis. Virions consistently concentrated in only one or two consecutive fractions, corresponding to a visible band in the gradient. Those fractions were dialyzed against buffer and stored at either 4°C or −80°C before use.

SDS-PAGE of purified virions showed a major Coomassie-stained band near the 80-kDa marker, consistent with a sequence-predicted mass of 75 kDa for TVV1-UH9 CP (8) (Fig. 1B). In overloaded lanes, a minor band was also routinely visible near the 160-kDa marker, consistent with a sequence-predicted mass of 160 kDa for the TVV1-UH9 CP/RdRp fusion product (8). The identity of this minor band was confirmed by tandem mass spectrometry of tryptic peptides (Fig. 2; also see next paragraph), as well as by immunoblotting with a polyclonal antiserum raised against a portion of the RdRp region (Fig. 1B, lane 3). Agarose gels of purified virions showed a major, ethidium-stained band migrating near the 5-kbp marker, consistent with a sequence length of 4.7 kbp for the TVV1-UH9 dsRNA genome (8) (Fig. 1C).

The plus-strand RNA (mRNA) of all of the TVV1 strains sequence characterized to date has a downstream RdRp ORF in the +1 frame relative to a partially overlapping upstream CP ORF (8, 10, 23, 24). The CP/RdRp fusion protein could therefore be most simply generated by a single, either +1 or −2, ribosomal frameshifting event (23, 24). Both +1 and −2 ribosomal frameshifts have been demonstrated in other organisms (29–34), though neither as commonly as a −1 frameshift (35, 36). Tandem mass spectrometry to confirm the identity of the CP/RdRp band from purified TVV1-UH9 virions allowed us to begin to address the frameshifting mechanism by identifying the tryptic peptide that spans the CP/RdRp junction. The identified peptide, VGSLFLSK (Fig. 2A; see Fig. S1 in the supplemental material), is consistent with −2, and not +1, frameshifting (Fig. 2B), and alternative peptides consistent with +1 frameshifting were not found. Thus, TVV1-UH9 appears to translate its CP/RdRp fusion product via −2 ribosomal frameshifting.

To further evaluate the virion preparations, we negatively stained and viewed them by TEM. The particles were seen to be well distributed, with limited clumping or breakage, and consistent widths near 400 Å (Fig. 3A). Most displayed an angular, almost hexagonal, profile. Moreover, the outer surfaces appeared to be uneven, with short but wide protrusions. Essentially all of the particles appeared to have been penetrated by stain. However, a few were penetrated much more than others and were interpreted as "empty" particles missing the dsRNA genome from their centers. Similar findings were obtained for purified virions that had been stored at 4°C for several days or at −80°C for several weeks before analysis. With longer storage at 4°C, or after even brief storage at −20°C, however, the incidence of clumped, broken, and empty particles increased, suggesting that purified TVV1 virions are relatively unstable.

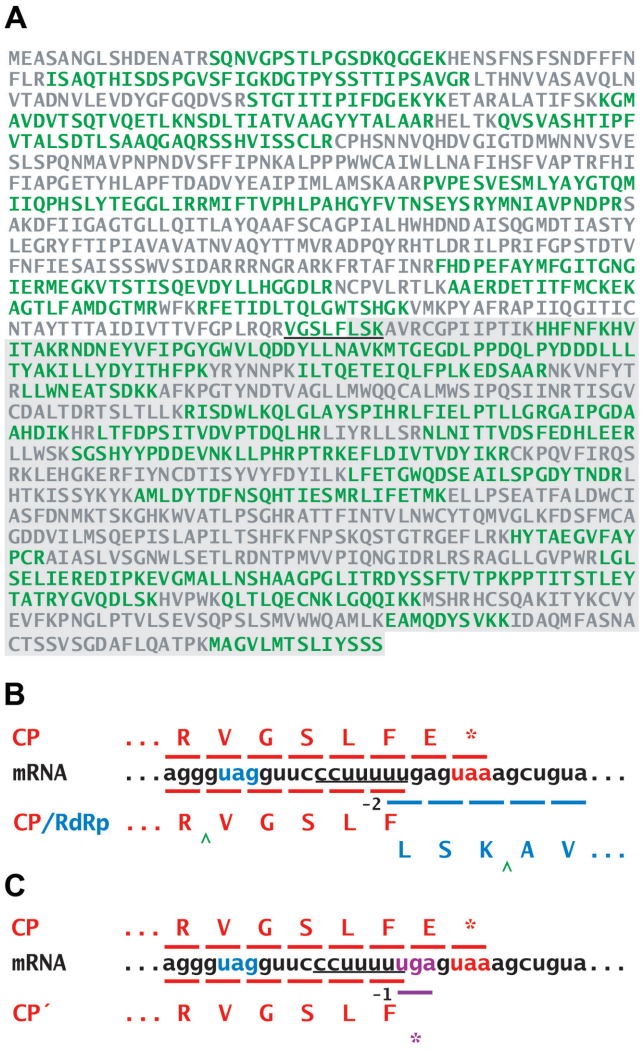

FIG 2 Mass spectrometry of TVV1-UH9 CP/RdRp and frameshifting models. (A) Tryptic peptides identified by LC/MS/MS are shown in green in the CP/RdRp sequence of TVV1-UH9. Residues in CP/RdRp derived from the RdRp ORF have gray background shading. The junctional peptide identified by LC-MS/MS is underlined and is consistent with a −2, and not a +1, frameshifting mechanism. (B) The mRNA sequence of TVV1-UH9 in the region of the CP/RdRp frameshift is shown in the middle in lowercase. All nucleotides are black, except for the stop codon defining the upstream end of the RdRp ORF (frame −2), which is blue, and the stop codon defining the downstream end of the CP ORF (frame 0), which is red. The putative slippery sequence is underlined. Frame 0 coding of CP is shown at the top. CP codons are overlined in red, and the encoded amino acid residues are shown in red type. Frame 0/−2 coding of CP/RdRp is shown at the bottom. CP codons are underlined in red, and the encoded amino acid residues are shown in red type; RdRp codons are underlined in blue, and the encoded amino acid residues are shown in blue type. Frameshift is labeled −2. Sites of trypsin cleavage of CP/RdRp to generate the identified junctional peptide are shown by green carets. (C) Same diagram as in panel B, except that the frame −1 stop codon in the mRNA sequence is purple, the frame 0/−1 coding of putative product CP′ is shown at the bottom, and the frameshift is labeled −1. The asterisks in panels B and C indicate stop codons.

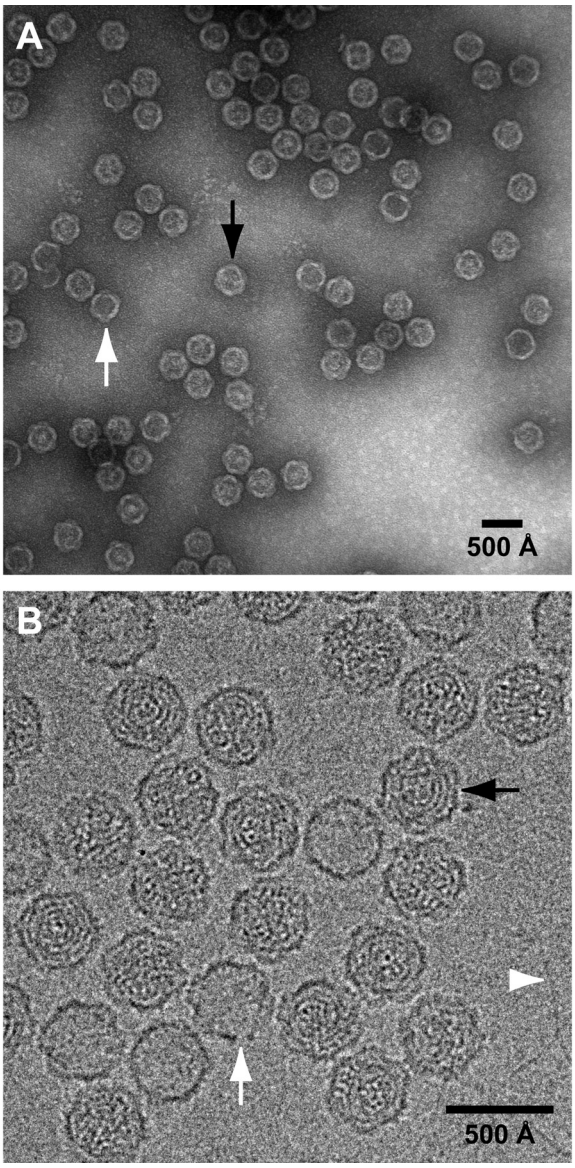

FIG 3 Electron micrographs of purified TVV1-UH9. Before microscopy, particles were either contrasted with uranyl formate (A) or vitrified and left unstained (B). In both panels, examples of full and empty TVV1 particles are indicated by black and white arrows, respectively. Many of the full particles in panel B show the presence of internal, arc-like densities, interpreted as genome. The white arrowhead in panel B points to a putative strand of free dsRNA in the solvent background.

Cryo-TEM of TVV1 virions. Virions analyzed by cryo-TEM were flash frozen on grids within 2 to 3 days of purification and storage at 4°C. Early preparations had lower concentrations warranting the use of continuous carbon grids. Though over 390 micrographs were captured from those grids, with ~3,100 particles boxed, resolutions of several 3D reconstructions were limited to ~11 Å or worse. A later preparation, however, was sufficiently concentrated for the use of holey carbon grids, and data collected from that preparation were used to extend the resolution.

Several features of the virions were again apparent in raw images, corroborating results of negative staining. Most particles had central densities attributable to the dsRNA genome, often in the form of fingerprint patterns (Fig. 3B). A few particles appeared to lack central densities, however, and consistent with loss of the genome from some such particles, linear strands suggestive of free dsRNA were seen at places in the solvent background. Most of the particles, both "full" and "empty," exhibited an angular outline, and many showed short but wide protrusions around the periphery. In fact, in a number of particles, six of these protrusions were seen, suggesting that they are centered at the capsid's icosahedral 5-fold (I5) axes and that particles with six of these visible protrusions are sitting with an I2 axis approximately facing the viewer.

3D reconstruction of TVV1 virions. An icosahedral image reconstruction of TVV1 virions (Fig. 4) was computed from 4,291 particle images recorded on 84 micrographs at a nominal magnification of ×59,000 in an FEI Polara microscope at 200,000 eV under minimal-dose conditions. The resolution of the map was estimated at 6.7 to 5.5 Å according to Fourier shell correlation (FSC) criteria (37), with a further voxelwise analysis indicating resolutions between 6.5 and 5.5 Å in different capsid regions.

The outermost diameter of the TVV1 virion is ~450 Å at positions surrounding the I5 axes, but the surface is quite uneven, with low points at diameters of ~375 Å near the I2 and I3 axes (Fig. 4A to C). The surface topography therefore comprises 12 pentameric plateaus, centered at the I5 axes and separated by a continuous network of canyons that connect the I2 and I3 axes. Upon closer inspection, each of the plateaus was seen to include 10, rather than 5, ovoid elements, with 5 (A) approaching the I5 axis and the other 5 (B) inserted partially between them. In the whole capsid, there are thus 60 A and 60 B elements, for a total of 120 representing the 120 CP subunits expected for a *Totiviridae* family member (38–41). Such capsids with 120 subunits have been nicknamed "$T = 2$" but have $T = 1$ symmetry with the icosahedral asymmetric unit (IAU) comprising an AB dimer.

Density projection images representing thin planar sections through the 3D map provide edge-on views of the capsid and reveal an inner surface smoother than the outer (Fig. 4A is an equatorial section of this type). Thinner regions of the capsid are visible near the I2 and I3 axes, reflecting the surface canyons, and thicker regions are visible near the I5 axes, reflecting the plateaus. Throughout these different regions are both punctate and elongated features (Fig. 4A) representing secondary-structure elements. Of particular note in the equatorial section are open channels at the I5 axes, ~20 Å wide, that span the full capsid thickness and appear larger than comparable ones found in other dsRNA viruses. The I5 channels are also visible in surface views (Fig. 4B) and in density projection images representing thin radial sections through the map (Fig. 4C). In surface views directly down an I5 axis, the channels are especially evident and appear wider than those in the genus *Totivirus* prototype Saccharomyces cerevisiae virus L-A (ScV-L-A) (see Fig. S2 in the supplemental material). Our conservative estimates of the I5 channel width in the current TVV1 structure (see Materials and Methods) are 16 Å near the bottom of the channel and 24 Å near the top of the channel, versus 14 Å for the channels in the resolution-matched structure of ScV-L-A (see Fig. S2; reported as 18 Å in the 3.3-Å ScV-L-A crystal structure [40]). Thus, even in TVV1, these channels are probably not directly large enough to allow escape of the dsRNA genome (26-Å diameter) or entry of most types of cellular proteins that might damage the genome (e.g., RNases). Secondary-structure elements, noted in Fig. 4A, are also seen in the radial sections, some dramatically so, such as two apparent α-helices that have

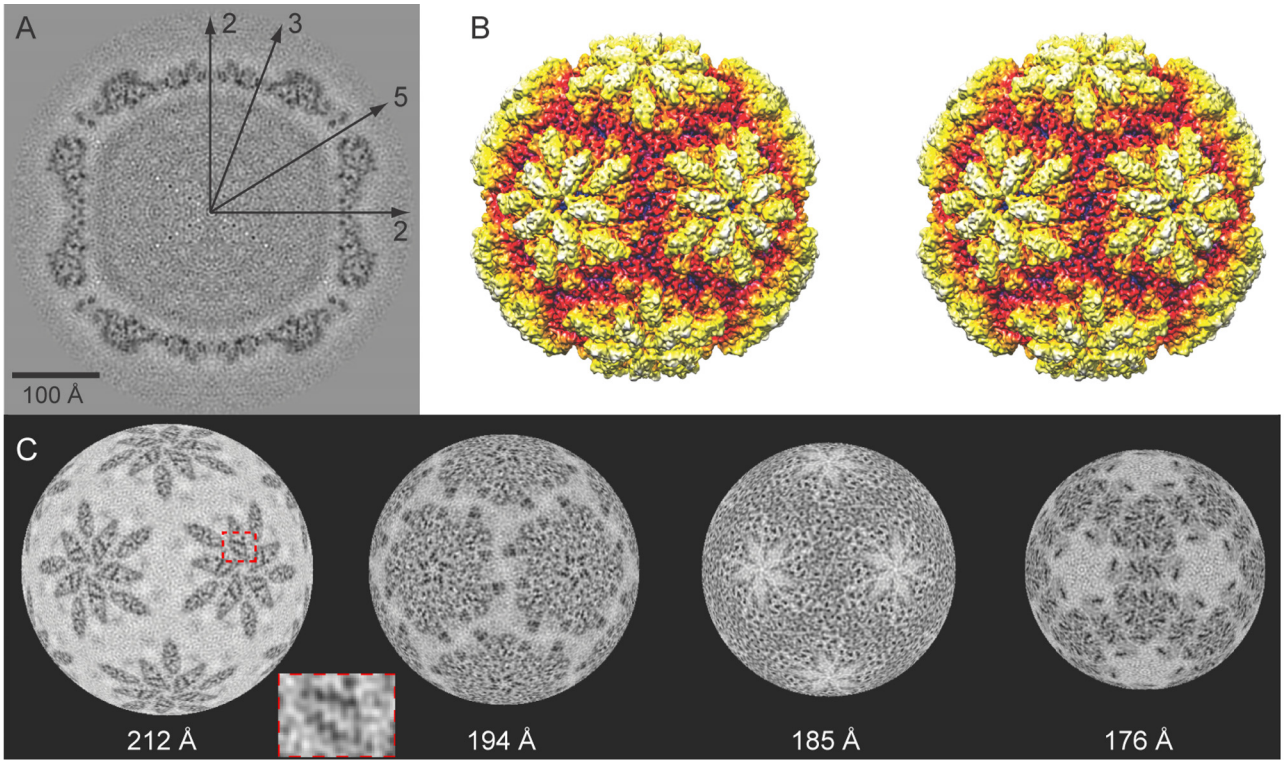

FIG 4 Icosahedral 3D image reconstruction of TVV1-UH9 virions. (A) Planar section through the particle, centered at the equator and 1 pixel (1.09 Å) thick. The map is coded in grayscale according to projected density (white, low; black, high). Icosahedral symmetry axes are marked (2, 3, and 5). (B) Space-filling view of the particle surface, in stereo, as viewed down an I2 axis. The map is color coded by radius (white, outermost; dark blue, innermost; see Fig. 6C for complete color legend). (C) Radial sections through the capsid, centered at indicated radii and each 1 pixel (1.09 Å) thick. The map is coded in grayscale as in panel A. Examples of characteristic, zigzag-shaped density features, corresponding to two putative α-helices, are highlighted (dashed red box) in the leftmost image and shown enlarged in the inset.

been fortuitously captured lengthwise and are represented by zigzag densities in the leftmost image of Fig. 4C and the inset therein.

Less-well-resolved densities in central regions of the equatorial section (Fig. 4A) are likely to represent the dsRNA genome. These densities take the form of two or three concentric rings, the outer one best resolved and each separated by ~30 Å (Fig. 5A and B). These rings are consistent with close packing of dsRNA helices into locally parallel arrays that are evenly distributed, on average, through open space in the particle interior. A similar arrangement has been described for other dsRNA viruses (42–44) and was first shown for double-stranded DNA (dsDNA) bacteriophages (45). The closest approaches between the capsid and outer RNA ring appear to occur near and flanking the I2 axes. Such contacts are likely important for determining the position of the outer ring and might also play roles in RNA packaging or transcription. In this regard, it is notable that the outer ring, in particular, has a hexagonal appearance in Fig. 4A, suggesting that it follows the capsid symmetry and is likely influenced by direct interactions with the capsid undersurface. Thickening of the outer-ring densities under the capsid I5 axes might reflect the presence of the RdRp domain hanging into the particle interior near those positions and representing the 1 or 2 CP/RdRp molecules thought to be present in each virion. The RdRp-associated densities in TVV1 are expected to be much weaker than those observed in *Reoviridae* family members (46, 47), which have 9 to 12 RdRp molecules packaged per virion.

3D reconstruction of TVV1 empty particles. During microscopy as noted above, we observed a subset of particles that seemed to be missing the genome, and we also observed some background dsRNA strands suggesting release from virions during storage or cryopreparation. We therefore separately boxed images of these "empty" particles and performed an icosahedral image reconstruction of them alone (Fig. 5). This reconstruction was computed from 1,416 particle images obtained from 82 of the same 84 micrographs as virions and reached an estimated resolution of 8.6 to 7.5 Å according to FSC criteria (37).

The 3D structure of "empties" appears very similar to that of virions, except that it lacks the central densities ascribed to dsRNA. The similarities and differences are evident in side-by-side comparisons of density projection images of planar equatorial sections of empties and virions (Fig. 5A), as well as in radial density plots averaged over the maps (Fig. 5B). Some subtle differences in the capsids become apparent, however, when images of virions and empties are rapidly alternated (see Movie S1 in the supplemental material), with a few features near the capsid-RNA interface appearing to have "breathed" slightly outward ($\leq$5 Å) in empties. These findings suggest that packaged dsRNA has evident, but limited, effects on capsid structure after the capsid has been formed but do not rule out the possibility that RNA has greater effects during capsid assembly.

There are several possibilities for how the genome exited purified virions with so little change in the capsid, including (i) revers-

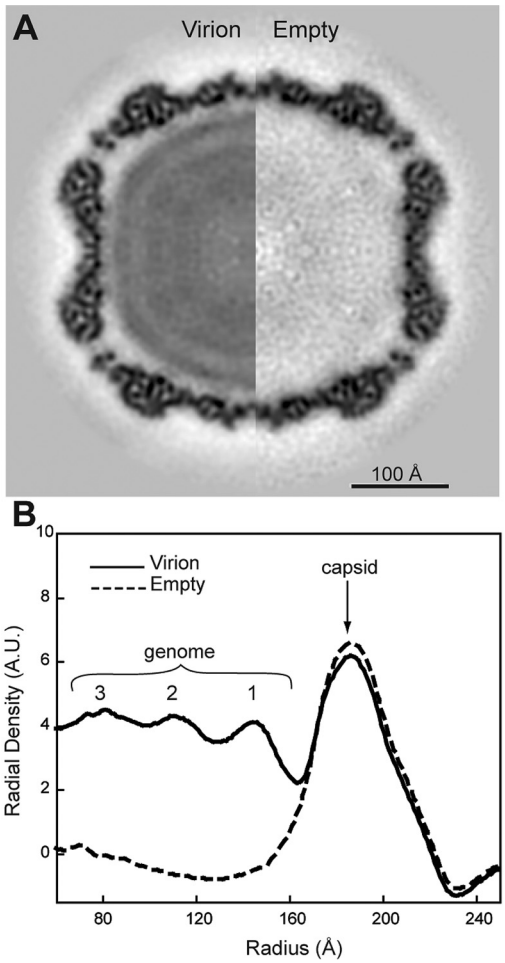

FIG 5 Comparison of TVV1 virion and empty capsid reconstructions. (A) Equatorial density section (1 pixel, representing a 1.09-Å thickness) through the TVV1 virion (left half) and empty capsid (right half) cryoreconstructions. For this comparison, both 3D maps were rendered at 8.6-Å resolution, which corresponds to the estimated resolution limit (at an FSC of 0.5) of the empty capsid. The highest- and lowest-density features are rendered in black and white, respectively. (B) Radial density plots of virions (solid line) and empty capsids (dashed line). Peaks corresponding to the capsid and three genome shells are labeled. Radial density is plotted in arbitrary units (A.U.).

ible changes and (ii) irreversible changes that were nonetheless small enough to be obscured during averaging for the icosahedral reconstruction. Given the unusually large width of the I5 channels in TVV1 (16 to 24 Å in the current structure), we propose that dsRNA exit is likely to have involved further expansion of one of these preexisting channels. Limited or transient exposure of the dsRNA through such expanded channels might also occur in intact virions, but only to an extent that maintains its resistance to RNase III cleavage (39), as we have recently reported for TVV1-UH9 virions (22).

Subunit arrangements in the TVV1 capsid. Ovoid elements surrounding the I5 axes in surface views of the capsid (Fig. 4B) appear to represent 120 CP subunits of two types, A and B. To assign specific features in more detail, we used an *ab initio* approach to segment out the densities attributable to each subunit in the 3D map (see Materials and Methods). Importantly, secondary-structure elements similar in shape and placement were observed as repeating units in both A and B, allowing us to distinguish those subunits. Using this approach, we produced a complete "$T = 2$" model that accounted for all of the capsid densities in the reconstruction (Fig. 6A). As seen for other *Totiviridae* family members (38–41), the A and B subunits in TVV1 appear to have similar overall density envelopes despite different local environments (Fig. 6A). Each displays an elongated, comma-like shape with the thickened end distal to the I5 axis. A subunits approach and surround each I5 axis, excluding B subunits, and B subunits approach and surround each I3 axis, excluding A subunits (Fig. 6A). In addition, A subunits from two different pentamers approach each other across each I2 axis, appearing to exclude B subunits from that axis as well.

Having assigned specific densities to A and B subunits, we found it instructive to examine them in pairs, since an AB dimer may be the protomer for capsid assembly. For any A subunit in the TVV1 capsid, there are three contacting B subunits, each with a distinct A-B interface. Two of the resulting dimers are asymmetric, whereas the third is quasisymmetric (respectively labeled AB_1, AB_2, and AB_3 in Fig. 6A). In other *Totiviridae* family members, as well as in larger dsRNA viruses from the family *Reoviridae*, one or the other asymmetric AB dimer has been picked to represent the IAU of the capsid (38, 39, 41, 48). The rationale for this choice has been the greater buried surface area, or compactness, in either asymmetric dimer than that of the quasisymmetric one. Another reason is that an assembly model has developed for *Reoviridae* family members in which a compact $(AB)_5$ decamer is a suggested intermediate (Fig. 6B), 12 of which are thought to combine to form the inner capsid (48–50). Applying that model to TVV1, the putative AB protomer would be one of the asymmetric dimers (AB_1 or AB_2 in Fig. 6A); it could not be the quasisymmetric one (AB_3) because the subunits in that dimer belong to two different compact decamers in the capsid (Fig. 6B). Another possibility, however, is that the putative decamer is less compact, comprising five A subunits interacting around the I5 axis and five quasisymmetrically placed B subunits hanging off as arms (Fig. 6C). Thus, a quasisymmetric AB protomer is also consistent with a decamer intermediate, albeit an unlikely one that is distinct from that previously suggested for *Reoviridae* family members (48–50). Interestingly, recent demonstrations of domain swapping within the quasisymmetric AB dimer of smaller dsRNA viruses from the families *Partitiviridae* and *Picobirnaviridae* (44, 51, 52) identify it as the more likely protomer of those viruses. Moreover, in those smaller viruses, as well as in larger viruses of the family *Cystoviridae* (53), an $(AB)_2$ tetramer intermediate is suspected or known to occur (44, 51–53), inconsistent with either type of decamer intermediate because subunits in the implicated tetramer belong to two different decamers in the capsid (Fig. 6D).

Returning to TVV1, there is no published evidence of a particular type of assembly intermediate for it or any other *Totiviridae* family member. Also, the A and B subunits in the ScV-L-A crystal structure at a 3.3-Å resolution do not show domain swapping (40) and thus do not indicate directly which AB dimer is the probable protomer. In the absence of such direct evidence, we therefore chose to identify one of the asymmetric dimers as the IAU of TVV1-UH9, specifically, the AB_1 dimer shown in Fig. 6A. Our main justification is that it is the only AB dimer consistent with either type of compact assembly intermediate, decamer or tetramer. The other asymmetric dimer (AB_2) is inconsistent with a

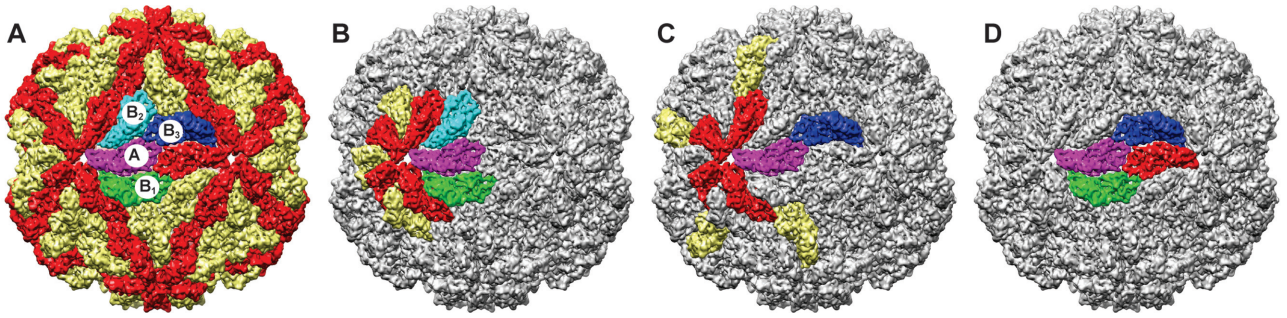

FIG 6 Segmentation of the TVV1-UH9 capsid and possible assembly intermediates. (A) Densities corresponding to A and B subunits according to segmentation analysis are, respectively, colored red and yellow, except for a chosen A subunit, which is colored purple, and the three B subunits that contact it, which are, respectively, colored green, cyan, and blue (B_1, B_2, and B_3). (B to D) Three possible assembly intermediates are shown: compact decamer (B), extended decamer (C), and compact tetramer (D). Only the A and B subunits within each intermediate are colored, in accordance with the scheme used in panel A.

compact tetramer, and the quasisymmetric dimer (AB_3) is inconsistent with a compact decamer (Fig. 6B and D).

Conserved structural elements in TVV1 and other *Totiviridae* family members. The arrangement of subunits in TVV1 is highly similar to that in ScV-L-A. To illustrate this point, we used rigid-body fitting with Chimera (54) to position the crystallography-derived atomic model of the designated IAU of ScV-L-A (Protein Data Bank 1M1C) (40) into an analogous AB dimer in the TVV1-UH9 map (Fig. 7A). The results demonstrate that the overall shapes of the density envelopes match very well and the angles between the A and B subunits are nearly identical, indicating that ScV-L-A and TVV1 have a strikingly conserved capsid organization. This organization is also quite like that in the capsids of the *Totiviridae* family member Helminthosporium vic-

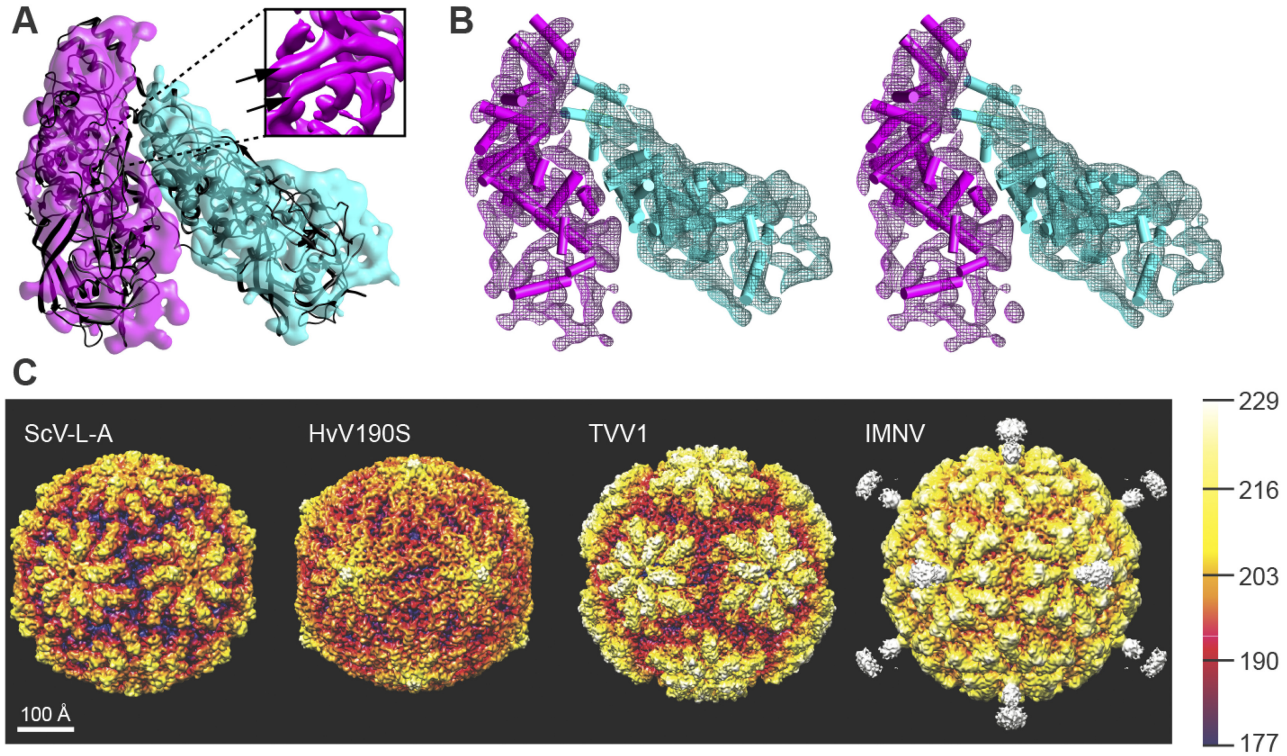

FIG 7 Comparisons of TVV1-UH9 and other *Totiviridae* family members. (A) The crystallography-derived atomic model of the asymmetric AB dimer of ScV-L-A (ribbon diagram in black) was fitted into segmented densities of the comparable dimer of TVV1-UH9 (partially transparent, space-filling model). The A and B subunit densities of TVV1-UH9 are colored magenta and cyan, respectively, to indicate their correspondence to the AB_2 dimer in Fig. 6A (rotated about 90° clockwise). The inset shows an enlarged area of subunit A viewed from the opposite side (rotated 180° about the vertical axis), which has been contoured at a slightly higher density level to highlight some of the tubular density features that we ascribe to α-helices (arrows identify two parallel helices). (B) Superimposed AB dimers of ScV-L-A and TVV1-UH9 shown in the same orientation as in panel A but in this case with both in stereo; with only the α-helices of ScV-L-A included, shown as magenta or cyan cylinders; and with TVV1-UH9 shown as density nets. (C) Space-filling view of the particle surface as viewed down an I2 axis of each respective virus. Each map is color coded by radius (Å) according to the scale at the right. The ScV-L-A structure is shown as simulated density at ~7-Å resolution derived from its 3.3-Å crystal structure (40), whereas the others are shown at 6.7 Å (TVV1) or ~7 Å (HvV190S and IMNV) from their respective cryo-TEM maps.

toriae virus 190S (HvV190S) (41) and the tentatively assigned member penaeid shrimp infectious myonecrosis virus (IMNV) (43) (Fig. 7C), as well as in the inner capsids of *Reoviridae* family members (42, 48, 49).

At the current resolution of the TVV1 map, we can identify numerous α-helices as twisted, tubular densities in both the A and B subunits, even though the map is not sufficiently resolved to trace the entire peptide backbone of either. The CPs of many *Totiviridae* family members seem to share a helical core (41). We therefore compared the 3D locations of putative helices in the TVV1 map to known helices in the ScV-L-A atomic model (40). Most of the helices in TVV1 do not strongly overlap ones in ScV-L-A, though several appear to have been only rotated or translated to nearby locations (Fig. 7B). Moreover, when we superimposed the segmented densities of one subunit each from TVV1 and HvV190S (41), we found that two putative, long "core" helices of the two CPs overlap quite well. It thus seems reasonable to conclude that the CPs of both fungal and protozoan *Totiviridae* family members have in common a helix-rich fold probably derived from an ancient common ancestor. Despite similar density envelopes and apparently similar helix-rich folds, however, identity scores in pairwise alignments of TVV1-UH9, ScV-L-A, and HvV190S CPs are quite low, <18% in each case (determined using EMBOSS Stretcher with default settings at http://www.ebi.ac.uk/Tools/psa/). Thus, the capacity for self-assembly into similarly organized capsids has been maintained despite extensive primary sequence divergence.

DISCUSSION

Phylogenetics and transmission strategies. The family *Totiviridae* comprises encapsidated dsRNA viruses with monosegmented genomes. The best-characterized members infect either fungi (*Ascomycota* and *Basidiomycota*) or protozoa (e.g., *Giardia*, *Leishmania*, and *Trichomonas*). TVV1 represents the fourth recognized virus of the family *Totiviridae* for which a 3D structure has been reported (38–41) and the first of the protozoan viruses to be thus characterized (see Fig. S3 in the supplemental material). A structure for penaeid shrimp IMNV has also been reported (43), but that virus remains only tentatively assigned to the family *Totiviridae*. Indeed, IMNV and other recently discovered, monosegmented dsRNA viruses from insects and fish (55, 56), all of which cluster with Giardia lamblia virus in sequence-based phylogenetic trees (see Fig. S3), remain to be formally classified and might be better placed in a new family or subfamily of more divergent monosegmented viruses that mediate extracellular transmission between hosts (43), unlike TVV1 and other *Totiviridae* family members.

That viruses such as TVV1 lack inherent means for extracellular transmission means that they lack virion-associated machinery for cell entry. It may also mean that they need not be as stable as many extracellularly transmitting viruses are, since they have no regular need to survive in varied environments outside cells. Some viruses with this transmission strategy have evolved to lack capsids, such as members of the family *Hypoviridae* (57), but others possess capsids, including TVV1 and members of several other dsRNA virus families. In these viruses, the capsid is essential in part because of their RNA replication strategy, which involves a capsid-associated RdRp and also in part because the capsid sequesters the genome and thereby reduces host sensing of dsRNA for associated responses in many hosts. The capsids of these viruses may also have other functions, such as in intracellular localization to promote partitioning into both daughter cells during cytokinesis or into the partner cell during mating. Nonetheless, their capsids have had no need to evolve functions for entering cells from the outside, such as cell surface receptor binding and membrane penetration. Thus, the complex surface topography of the TVV1 virion seen in this study is almost certainly unrelated to any functions for entering *T. vaginalis* cells from the extracellular environment.

Contribution of TVV1 and other TVVs to human trichomoniasis and its complications. An important reason for wishing to have a more complete understanding of protozoan viruses includes recent evidence that both LRV1 and TVVs determine important mammalian responses to the respective protozoan infections, in a mouse model for LRV1 and a human cell model for TVVs (21, 22). In fact, for TVVs, our recent results with the antiprotozoan drug metronidazole suggest that virions escaping from damaged or dying *T. vaginalis* cells might be sensed by human epithelial cells, leading to the upregulation of immunoinflammatory cytokines and chemokines via dsRNA-dependent signaling pathways and exacerbation of disease symptoms (22). This and other evidence of the role of virions provided special incentive for the present study to determine the 3D structure of TVV1. As described in Results, the newly observed, wide I5 channels might contribute to effects on human cells by facilitating the release of the dsRNA genome, which is then sensed by the human cells endosomally (22). On the basis of the behavior of *T. vaginalis* isolate UH9 and purified TVV1-UH9 virions in inducing immunoinflammatory signaling (22), we conclude that TVV1 is sufficient for these effects on human epithelial cells, but we do not yet know if it is necessary. Perhaps TVV2, TVV3, and TVV4 can contribute as well, and perhaps even in distinct manners.

Important questions remain about precisely how TVV1 virions, and perhaps those of other TVVs, interact with human cells, first at the plasma membrane and then along one or more endocytic pathways, to determine the observed immunoinflammatory responses that contribute to the pathogenesis of human trichomoniasis and its complications (1). One possibility, for example, is that extracellular or endosomal proteases may digest the TVV capsid and provide even greater exposure or release of the viral dsRNA. Which endocytic uptake pathway may contribute most to these effects is also important to determine.

Ribosomal frameshifting in TVV1. Examples of −1 programmed ribosomal frameshifting are widely distributed and appear in most cases to use a similarly specified mechanism involving a 7-nucleotide RNA slippery sequence, X-XXY-YYZ (dashes indicate codon breaks in frame 0), and a nearby downstream RNA structure, often a pseudoknot (35, 36). The RNA structure causes ribosomal pausing, which stimulates the ribosome to slide back one base at the end of the slippery sequence and then read ZNN as the next codon. The TVV2, TVV3, and TVV4 strains probably use a related such mechanism to express their CP/RdRp fusions, in that the downstream RdRp ORF overlaps the upstream CP ORF in the −1 frame and also an RNA "slippery-like" sequence (G-GGC-CCC in TVV2, G-GGC-CCU in TVV3 and TVV4) is conserved within this overlap (8, 10).

In TVV1 strains such as TVV1-UH9, on the contrary, the downstream RdRp ORF overlaps the upstream CP ORF in the +1 frame, so a different program of ribosomal frameshifting is required, even though a putative RNA "slippery-like" sequence (C-

CUU-UUU) is conserved within the overlap (8, 10, 23, 24). The overlap between the CP and RdRp ORFs in TVV1 strains is short, only 14 nucleotides between flanking stop codons (Fig. 2B), restricting the necessary frameshift to this small region that includes the putative slippery motif. Shifting of translation to the +1 frame can occur by a single, either +1 or −2, ribosomal frameshifting event, though until recently, −2 frameshifting had been shown to be used naturally by only one organism, dsDNA bacteriophage Mu (31), to express a C-terminally extended form of one of its tail assembly proteins, and to occur after genetic manipulations of two others, HIV-1 and budding yeast (32, 33). Recently, though, −2 frameshifting has been shown to be used naturally by mammalian arteriviruses, plus-stranded RNA viruses related to coronaviruses and including the important swine pathogen porcine reproductive and respiratory syndrome virus, to express a C-terminally extended form of one of their nonstructural proteins (34). The authors of the arterivirus report have further predicted, on the basis of sequence features, that −2 frameshifting is likely also to be used by TVV1 (34, 36). The demonstration here that the junctional peptide of TVV1-UH9 CP/RdRp is consistent with −2, and not +1, frameshifting agrees with that prediction. In the arteriviruses, the −2 slippery motif has been identified as G-GUU-UUU, at the end of which the ribosome slides back two bases, reading UUN as the next codon, which is in line with the −2 slippery motif of TVV1, C-CUU-UUU (Fig. 2B). Since it is an uncommonly found mechanism to date, perhaps −2 frameshifting by TVV1 could be a target for novel antiviral compounds that would clear *T. vaginalis* cells of TVV1 without damaging the protozoan and thereby leading to enhanced immunoinflammatory signaling by human epithelial cells, as metronidazole has been shown to do (22).

It is also interesting to note what would happen should the ribosome slide back only one base (i.e., undergo a −1 frameshift) at the end of the TVV1 slippery sequence, as has been shown to occur at the arterivirus slippery sequence, albeit at lower frequency than −2 frameshifting (34). In every sequence-characterized TVV1 strain to date, a −1 frameshift on this slippery sequence would lead the ribosome to immediately encounter a conserved stop codon, UGA (8, 10). Thus, a −1 frameshift would yield an alternative version of CP that is a single Glu residue shorter than the nonframeshifted product (Fig. 2C). Given its possible significance, we have attempted to demonstrate this second form of CP, but so far with no success.

MATERIALS AND METHODS

***T. vaginalis* culture.** *T. vaginalis* isolate UH9 (8) was grown in iron-supplemented Diamond's TYM medium (pH 6.0) with 10% horse serum at 37°C without shaking and with the screw-cap culture tube tightly sealed to minimize gas exchange. The culture was passaged daily at late exponential phase and expanded to 2 liters as necessary for TVV purification.

TVV1 purification. TVV1-UH9 virions were purified as previously described (12), though with some modifications. Cells from the *T. vaginalis* culture were sonicated in high-salt buffer (2.15 M NaCl, 10 mM phosphate buffer, pH 7.2) in the presence of protease inhibitor cocktail (Roche). After being cleared of debris by centrifugation (10,000 × *g*, 30 min, 4°C), the lysate was pelleted through a 40% sucrose cushion (230,000 × *g*, 2 h, 4°C). Pelleted material was then resuspended in HN buffer (50 mM HEPES [pH 7.2], 0.5 M NaCl) and separated in a CsCl density gradient (260,000 × *g*, 18 to 24 h, 4°C). The peak virion fractions, identified by SDS-PAGE, were dialyzed with HN buffer plus 20 mM $MgCl_2$. The concentrations of dialyzed preparations measured between 50 and 200 μg/ml by a modified Bradford assay (Bio-Rad). To check sample quality, purified TVV1-UH9 virions were examined by TEM after negative staining with uranyl formate. Aliquoted samples were stored at 4°C for up to 2 days or at −80°C until use.

Mass spectrometry. Purified TVV1-UH9 virions were disrupted and run on an 8% SDS-PAGE gel. After the gel was stained with Coomassie brilliant blue R-250 and then destained, the ~160-kDa CP/RdRp protein band was excised. The gel band was reduced with dithiothreitol, alkylated with iodoacetamide, and digested with sequencing grade trypsin. Extracted peptides were analyzed by reversed-phase (C_{18}) microcapillary liquid chromatography and tandem mass spectrometry (LC-MS/MS) with a high-resolution hybrid linear ion trap Orbitrap XL mass spectrometer (Thermo, Fisher Scientific) coupled to an EASY-nLC nanoflow high-performance liquid chromatograph (Thermo, Fisher Scientific). Spectra were analyzed with the Sequest search engine against a reversed and concatenated sequence database that was customized to contain all of the logically possible CP/RdRp proteins that could arise from different forms of frameshifting at different positions in the CP-RdRp overlap region. A fixed modification on Cys (+57.02) and variable modifications on Met (+15.99) and Asn/Gln (+0.98) were included in the search. A false discovery rate peptide threshold of 1% was used based on the Sp and Xcorr Sequest scores.

Cryo-TEM. Purified TVV1-UH9 virions were further concentrated by centrifugation through a 30,000-M_r filter (Amicon). Small (3.5-μl) aliquots of each sample were then vitrified and examined as previously described (58). Briefly, samples were applied to Quantifoil holey grids that had been glow discharged for ~15 s in an Emitech K350 evaporation unit. Grids were then blotted with Whatman filter paper for ~5 s, plunged into liquid ethane, and transferred into a precooled FEI Polara multispecimen holder, which kept the specimen at liquid nitrogen temperature. Micrographs were recorded on Kodak SO-163 electron image film in an FEI Polara microscope at 200,000 eV under minimal-dose conditions (~22 e/Å^2) at a nominal magnification of ×59,000 and with objective lens defocus settings ranging from 0.87 to 4.12 μm. Objective lens astigmatism was minimized during the microscope alignment procedure that preceded the recording of images and did not increase during the session in which all represented data were collected.

Icosahedral image reconstructions. Micrographs exhibiting minimal astigmatism and specimen drift were selected for processing and were digitized at 6.35-μm intervals (representing 1.09-Å pixels at the specimen) on a Nikon Supercoolscan 8000 microdensitometer. The program RobEM (http://cryoEM.ucsd.edu/programs.shtm) was used to estimate defocus and astigmatism, extract particle images, and preprocess the images as previously described (58). For each specimen, 150 particle images were used as the input for random-model computation to generate an initial 3D density map at an ~25-Å resolution (59). This map was then used to determine and refine particle orientations and origins for the complete set of images with AUTO3DEM v4.02 (60). Phases but not amplitudes of the structure factor data were corrected for effects caused by the microscope contrast transfer function (46, 61). After calculation of the FSC between two reconstructions generated from half data sets, FSC = 0.5 − 0.143 threshold criteria were used to estimate the resolution limit of each full data set (37). Before the calculation, a soft mask was applied to the two reconstructions to suppress most of the solvent. To generate the soft mask, the programs bfilter, bmask, and bsegment from Bsoft (http://lsbr.niams.nih.gov/bsoft/) were used. The original map was low-pass filtered to 15 Å (bfilter), and a binary mask was obtained by applying a threshold that visually included all of the densities in the shell (bmask). To eliminate contributions from the genome in virions, the mask was segmented into separate regions (bsegment), and only the shell region was retained (bmask). Finally, the binary mask was transformed into a soft mask by applying three iterations of an average filter with kernel size 3 (bfilter). For the virion map, an additional resolution estimate was performed, which analyzed the reconstruction in a localized manner, calculating the FSC around voxels of interest (blocres).

To aid our interpretations, we computed the final 3D maps with an inverse temperature factor of 250 Å^2 (62). Graphical representations were generated with RobEM and Chimera (54). The reconstructions were rendered at an isodensity contour level of 1.2 σ for space-filling views of the TVV1 surface (Fig. 4B, 6, and 7C; see Fig. S2 in the supplemental material). The width of the I5 channel was measured in Chimera while using a spherical marker for guidance. To assess the accuracy of the estimate, we repeated the measurement while changing the contour level between 1.0 and 1.5 σ, corresponding to a variation in capsid volume of ~20%. As a result, the channel width varied by <10%. Map segmentation was performed with the Segger tool (63) in Chimera as previously described (41). Briefly, the segmentation obtained with this tool does not rely on an initial model and was refined in a semiautomatic manner by imposing additional restrictions. Specifically, these restrictions ensured that global morphology and specific features were repeated in the A and B subunits, that the symmetry constraints of the icosahedral arrangement of subunits within the capsid were maintained, and that no obvious capsid density was left unassigned.

SUPPLEMENTAL MATERIAL

Supplemental material for this article may be found at http://mbio.asm.org/lookup/suppl/doi:10.1128/mBio.00056-13/-/DCSupplemental.

Movie S1, MOV file, 1.3 MB.
Figure S1, TIF file, 0.2 MB.
Figure S2, TIF file, 8.7 MB.
Figure S3, TIF file, 1.1 MB.

ACKNOWLEDGMENTS

We thank Bibhuti N. Singh for providing *T. vaginalis* UH9, Tomasz Kula for help with *T. vaginalis* culture, and Min Yuan and Susanne Breitkopf for assistance with mass spectrometry. We also acknowledge Andrew E. Firth for his correct prediction concerning TVV1 frameshifting (34, 36).

This work was supported by a Harvard Catalyst Pilot Grant (R.N.F., M.L.N.) through NIH grant UL1-RR025758 to the Harvard Clinical and Translational Science Center; by a Dana Farber/Harvard Cancer Center Support Grant (J.M.A.) through NIH grant P30-CA006516; by NIH grants P01-CA120964 (J.M.A.), R01-AI079085 (R.N.F.), RC1-AI086788 and R56-AI091889 (R.N.F., M.L.N.), and 1S10 RR020016 and R37-GM033050 (T.S.B.); and by UCSD and the Agouron Foundation (T.S.B.).

REFERENCES

1. **Fichorova RN.** 2009. Impact of *T. vaginalis* infection on innate immune responses and reproductive outcome. J. Reprod. Immunol. **83**:185–189.
2. **Schwebke JR, Burgess D.** 2004. Trichomoniasis. Clin. Microbiol. Rev. **17**:794–803.
3. **Wang AL, Wang CC.** 1986. The double-stranded RNA in *Trichomonas vaginalis* may originate from virus-like particles. Proc. Natl. Acad. Sci. U. S. A. **83**:7956–7960.
4. **Tai JH, Su HM, Tsai J, Shaio MF, Wang CC.** 1993. The divergence of Trichomonas vaginalis virus RNAs among various isolates of *Trichomonas vaginalis*. Exp. Parasitol. **76**:278–286.
5. **Wendel KA, Rompalo AM, Erbelding EJ, Chang TH, Alderete JF.** 2002. Double-stranded RNA viral infection of *Trichomonas vaginalis* infecting patients attending a sexually transmitted diseases clinic. J. Infect. Dis. **186**:558–561.
6. **Weber B, Mapeka TM, Maahlo MA, Hoosen AA.** 2003. Double stranded RNA virus in South African *Trichomonas vaginalis* isolates. J. Clin. Pathol. **56**:542–543.
7. **Fraga J, Rojas L, Sariego I, Fernández-Calienes A.** 2005. Double-stranded RNA viral infection in Cuban *Trichomonas vaginalis* isolates. Braz. J. Infect. Dis. **9**:521–524.
8. **Goodman RP, Freret TS, Kula T, Geller AM, Talkington MW, Tang-Fernandez V, Suciu O, Demidenko AA, Ghabrial SA, Beach DH, Singh BN, Fichorova RN, Nibert ML.** 2011. Clinical isolates of *Trichomonas vaginalis* concurrently infected by strains of up to four Trichomonasvirus species (family *Totiviridae*). J. Virol. **85**:4258–4270.
9. **Bessarab IN, Nakajima R, Liu HW, Tai JH.** 2011. Identification and characterization of a type III Trichomonas vaginalis virus in the protozoan pathogen *Trichomonas vaginalis*. Arch. Virol. **156**:285–294.
10. **Goodman RP, Ghabrial SA, Fichorova RN, Nibert ML.** 2011. *Trichomonasvirus*: a new genus of protozoan viruses in the family *Totiviridae*. Arch. Virol. **156**:171–179.
11. **Khoshnan A, Alderete JF.** 1993. Multiple double-stranded RNA segments are associated with virus particles infecting *Trichomonas vaginalis*. J. Virol. **67**:6950–6955.
12. **Bessarab IN, Liu HW, Ip CF, Tai JH.** 2000. The complete cDNA sequence of a type II Trichomonas vaginalis virus. Virology **267**:350–359.
13. **Fraga J, Rojas L, Sariego I, Fernández-Calienes A, Nuñez FA.** 2012. Species typing of Cuban Trichomonas vaginalis virus by RT-PCR, and association of TVV-2 with high parasite adhesion levels and high pathogenicity in patients. Arch. Virol. **157**:1789–1795.
14. **Wang AL, Wang CC.** 1986. Discovery of a specific double-stranded RNA virus in *Giardia lamblia*. Mol. Biochem. Parasitol. **21**:269–276.
15. **Tarr PI, Aline RF, Smiley BL, Scholler J, Keithly J, Stuart K.** 1988. LR1: a candidate RNA virus of *Leishmania*. Proc. Natl. Acad. Sci. U. S. A. **85**:9572–9575.
16. **Khramtsov NV, Woods KM, Nesterenko MV, Dykstra CC, Upton SJ.** 1997. Virus-like, double-stranded RNAs in the parasitic protozoan *Cryptosporidium parvum*. Mol. Microbiol. **26**:289–300.
17. **Wang A, Wang CC, Alderete JF.** 1987. *Trichomonas vaginalis* phenotypic variation occurs only among trichomonads infected with the double-stranded RNA virus. J. Exp. Med. **166**:142–150.
18. **Khoshnan A, Alderete JF.** 1994. *Trichomonas vaginalis* with a double-stranded RNA virus has upregulated levels of phenotypically variable immunogen mRNA. J. Virol. **68**:4035–4038.
19. **Provenzano D, Khoshnan A, Alderete JF.** 1997. Involvement of dsRNA virus in the protein composition and growth kinetics of host *Trichomonas vaginalis*. Arch. Virol. **142**:939–952.
20. **Fraga J, Rojas L, Sariego I, Fernandez-Calienes A, Nunez FA.** 2007. Double-stranded RNA viral infection of *Trichomonas vaginalis* and association with clinical presentation. Acta Protozool. **46**:93–98.
21. **Ives A, Ronet C, Prevel F, Ruzzante G, Fuertes-Marraco S, Schutz F, Zangger H, Revaz-Breton M, Lye LF, Hickerson SM, Beverley SM, Acha-Orbea H, Launois P, Fasel N, Masina S.** 2011. Leishmania RNA virus controls the severity of mucocutaneous leishmaniasis. Science **331**:775–778.
22. **Fichorova RN, Lee Y, Yamamoto HS, Takagi Y, Hayes GR, Goodman RP, Chepa-Lotrea X, Buck OR, Murray R, Kula T, Beach DH, Singh BN, Nibert ML.** 2012. Endobiont viruses sensed by the human host—beyond conventional antiparasitic therapy. PLoS One **7**:e48418. http://dx.doi.10.1371/journal.pone.0048418.
23. **Tai JH, Ip CF.** 1995. The cDNA sequence of Trichomonas vaginalis virus-T1 double-stranded RNA. Virology **206**:773–776.
24. **Su HM, Tai JH.** 1996. Genomic organization and sequence conservation in type I Trichomonas vaginalis viruses. Virology **222**:470–473.
25. **Liu HW, Chu YD, Tai JH.** 1998. Characterization of Trichomonas vaginalis virus proteins in the pathogenic protozoan *T. vaginalis*. Arch. Virol. **143**:963–970.
26. **Tai JH, Chang SC, Ip CF, Ong SJ.** 1995. Identification of a satellite double-stranded RNA in the parasitic protozoan *Trichomonas vaginalis* infected with T. vaginalis virus T1. Virology **208**:189–196.
27. **Fujimura T, Esteban R, Wickner RB.** 1986. In vitro L-A double-stranded RNA synthesis in virus-like particles from *Saccharomyces cerevisiae*. Proc. Natl. Acad. Sci. U. S. A. **83**:4433–4437.
28. **Malik SB, Pightling AW, Stefaniak LM, Schurko AM, Logsdon JM, Jr..** 2007. An expanded inventory of conserved meiotic genes provides evidence for sex in *Trichomonas vaginalis*. PLoS One **3**:e2879. http://dx.doi.10.1371/journal.pone.0002879.
29. **Belcourt MF, Farabaugh PJ.** 1990. Ribosomal frameshifting in the yeast retrotransposon Ty: tRNAs induce slippage on a 7 nucleotide minimal site. Cell **62**:339–352.
30. **Ivanov IP, Atkins JF.** 2007. Ribosomal frameshifting in decoding antizyme mRNAs from yeast and protists to humans: close to 300 cases reveal remarkable diversity despite underlying conservation. Nucleic Acids Res. **35**:1842–1858.
31. **Xu J, Hendrix RW, Duda RL.** 2004. Conserved translational frameshift in dsDNA bacteriophage tail assembly genes. Mol. Cell **16**:11–21.
32. **Matsufuji S, Matsufuji T, Wills NM, Gesteland RF, Atkins JF.** 1996. Reading two bases twice: mammalian antizyme frameshifting in yeast. EMBO J. **15**:1360–1370.

33. **Lin Z, Gilbert RJ, Brierley I.** 2012. Spacer-length dependence of programmed −1 or −2 ribosomal frameshifting on a U6A heptamer supports a role for messenger RNA (mRNA) tension in frameshifting. Nucleic Acids Res. **40**:8674–8689.
34. **Fang Y, Treffers EE, Li Y, Tas A, Sun Z, van der Meer Y, de Ru AH, van Veelen PA, Atkins JF, Snijder EJ, Firth AE.** 2012. Efficient −2 frameshifting by mammalian ribosomes to synthesize an additional arterivirus protein. Proc. Natl. Acad. Sci. U. S. A. **109**:E2920–E2928.
35. **Dinman JD.** 2012. Control of gene expression by translational recoding. Adv. Protein Chem. Struct. Biol. **86**:129–149.
36. **Firth AE, Brierley I.** 2012. Non-canonical translation in RNA viruses. J. Gen. Virol. **93**:1385–1409.
37. **Rosenthal PB, Henderson R.** 2003. Optimal determination of particle orientation, absolute hand, and contrast loss in single-particle electron cryomicroscopy. J. Mol. Biol. **333**:721–745.
38. **Cheng RH, Caston JR, Wang G-J, Gu F, Smith TJ, Baker TS, Bozarth RF, Trus BL, Cheng N, Wickner RB, Steven AC.** 1994. Fungal virus capsids, cytoplasmic compartments for the replication of double-stranded RNA, formed as icosahedral shells of asymmetric gag dimers. J. Mol. Biol. **244**:255–258.
39. **Castón JR, Trus BL, Booy FP, Wickner RB, Wall JS, Steven AC.** 1997. Structure of L-A virus: a specialized compartment for the transcription and replication of double-stranded RNA. J. Cell Biol. **138**:975–985.
40. **Naitow H, Tang J, Canady M, Wickner RB, Johnson JE.** 2002. L-A virus at 3.4 Å resolution reveals particle architecture and mRNA decapping mechanism. Nat. Struct. Biol. **9**:725–728.
41. **Dunn SE, Li H, Cardone G, Nibert ML, Ghabrial SA, Baker TS.** 2013. Three-dimensional structure of victorivirus HvV190S suggests coat proteins in most totiviruses share a conserved core. PLoS Pathog. **9**: e1003225. http://dx.doi.10.1371/journal.ppat.1003225.
42. **Reinisch KM, Nibert ML, Harrison SC.** 2000. Structure of the reovirus core at 3.6 Å resolution. Nature **404**:960–967.
43. **Tang J, Ochoa WF, Sinkovits RS, Poulos BT, Ghabrial SA, Lightner DV, Baker TS, Nibert ML.** 2008. Infectious myonecrosis virus has a totivirus-like, 120-subunit capsid, but with fiber complexes at the fivefold axes. Proc. Natl. Acad. Sci. U. S. A. **105**:17526–17531.
44. **Pan J, Dong L, Lin L, Ochoa WF, Sinkovits RS, Havens WM, Nibert ML, Baker TS, Ghabrial SA, Tao YJ.** 2009. Atomic structure reveals the unique capsid organization of a dsRNA virus. Proc. Natl. Acad. Sci. U. S. A. **106**:4225–4230.
45. **Earnshaw WC, Harrison SC.** 1977. DNA arrangement in isometric phage heads. Nature **268**:598–602.
46. **Zhang X, Walker SB, Chipman PR, Nibert ML, Baker TS.** 2003. Reovirus polymerase λ3 localized by cryo-electron microscopy of virions at a resolution of 7.6 A. Nat. Struct. Biol. **10**:1011–1018.
47. **Estrozi LF, Settembre EC, Goret G, McClain B, Zhang X, Chen JZ, Grigorieff N, Harrison SC.** 2013. Location of the dsRNA-dependent polymerase, VP1, in rotavirus particles. J. Mol. Biol. **425**:124–132.
48. **McClain B, Settembre E, Temple BR, Bellamy AR, Harrison SC.** 2010. X-ray crystal structure of the rotavirus inner capsid particle at 3.8 Å resolution. J. Mol. Biol. **397**:587–599.
49. **Grimes JM, Burroughs JN, Gouet P, Diprose JM, Malby R, Ziéntara S, Mertens PP, Stuart DI.** 1998. The atomic structure of the bluetongue virus core. Nature **395**:470–478.
50. **Kar AK, Ghosh M, Roy P.** 2004. Mapping the assembly pathway of bluetongue virus scaffolding protein VP3. Virology **324**:387–399.
51. **Ochoa WF, Havens WM, Sinkovits RS, Nibert ML, Ghabrial SA, Baker TS.** 2008. Partitivirus structure reveals a 120-subunit, helix-rich capsid with distinctive surface arches formed by quasisymmetric coat-protein dimers. Structure **16**:776–786.
52. **Duquerroy S, Da Costa B, Henry C, Vigouroux A, Libersou S, Lepault J, Navaza J, Delmas B, Rey FA.** 2009. The picobirnavirus crystal structure provides functional insights into virion assembly and cell entry. EMBO J. **28**:1655–1665.
53. **Kainov DE, Butcher SJ, Bamford DH, Tuma R.** 2003. Conserved intermediates on the assembly pathway of double-stranded RNA bacteriophages. J. Mol. Biol. **328**:791–804.
54. **Goddard TD, Huang CC, Ferrin TE.** 2007. Visualizing density maps with UCSF Chimera. J. Struct. Biol. **157**:281–287.
55. **Wu Q, Luo Y, Lu R, Lau N, Lai EC, Li WX, Ding SW.** 2010. Virus discovery by deep sequencing and assembly of virus-derived small silencing RNAs. Proc. Natl. Acad. Sci. U. S. A. **107**:1606–1611.
56. **Haugland O, Mikalsen AB, Nilsen P, Lindmo K, Thu BJ, Eliassen TM, Roos N, Rode M, Evensen O.** 2011. Cardiomyopathy syndrome of Atlantic salmon (*Salmo salar* L.) is caused by a double-stranded RNA virus of the *Totiviridae* family. J. Virol. **85**:5275–5286.
57. **Nuss DL.** 2005. Hypovirulence: mycoviruses at the fungal-plant interface. Nat. Rev. Microbiol. **3**:632–642.
58. **Baker TS, Olson NH, Fuller SD.** 1999. Adding the third dimension to virus life cycles: three-dimensional reconstruction of icosahedral viruses from cryo-electron micrographs. Microbiol. Mol. Biol. Rev. **63**:862–922.
59. **Yan X, Dryden KA, Tang J, Baker TS.** 2007. *Ab initio* random model method facilitates 3D reconstruction of icosahedral particles. J. Struct. Biol. **157**:211–225.
60. **Yan X, Sinkovits RS, Baker TS.** 2007. AUTO3DEM—an automated and high throughput program for image reconstruction of icosahedral particles. J. Struct. Biol. **157**:73–82.
61. **Bowman VD, Chase ES, Franz AW, Chipman PR, Zhang X, Perry KL, Baker TS, Smith TJ.** 2002. An antibody to the putative aphid recognition site on cucumber mosaic virus recognizes pentons but not hexons. J. Virol. **76**:12250–12258.
62. **Havelka WA, Henderson R, Oesterhelt D.** 1995. Three-dimensional structure of halorhodopsin at 7 Å resolution. J. Mol. Biol. **247**:726–738.
63. **Pintilie GD, Zhang J, Goddard TD, Chiu W, Gossard DC.** 2010. Quantitative analysis of cryo-EM density map segmentation by watershed and scale-space filtering, and fitting of structures by alignment to regions. J. Struct. Biol. **170**:427–438.